4）*In-vivo* においてマウス抗 II 型コラーゲン抗体カクテル関節炎モデルを用いて関節炎発症における MIF の関与を検討した。野生型（以下 WT）マウスは関節炎発症に伴い関節局所における MIF mRNA の発現が著しく増加し、また MMP-13（マウス MMP-1 ホモログ）および MIP-2（マウス IL-8 ホモログ）mRNA の発現も増加した。WT マウスに関節炎発症操作前に抗 MIF 抗体を投与した群（以下 MIF-Ab 群）および MIF ノックアウトマウス群（以下 MIF-KO 群）では、関節炎スコア（12 点満点）が WT 群で平均 7.6 点であったのに対し、MIF-Ab 群で平均 3.0 点、MIF-KO 群で平均 2.2 点と有意に関節炎が抑制され、これに伴い後者 2 群とも関節局所における MMP-13 および MIP-2 mRNA 発現、および炎症性細胞浸潤が抑制された（図４）。

図４

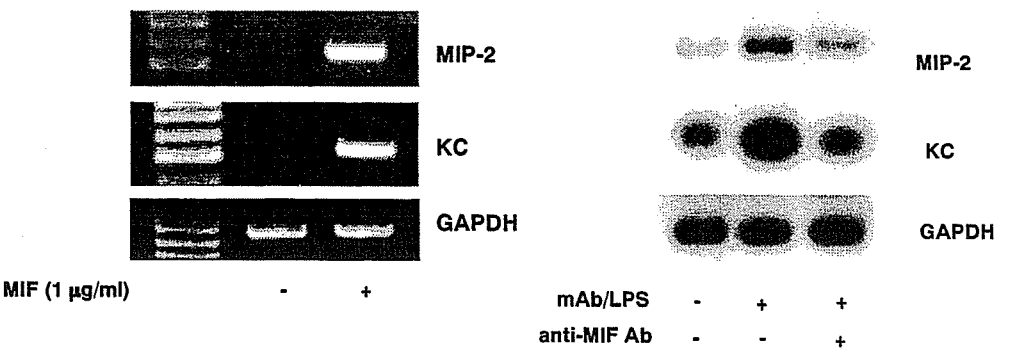

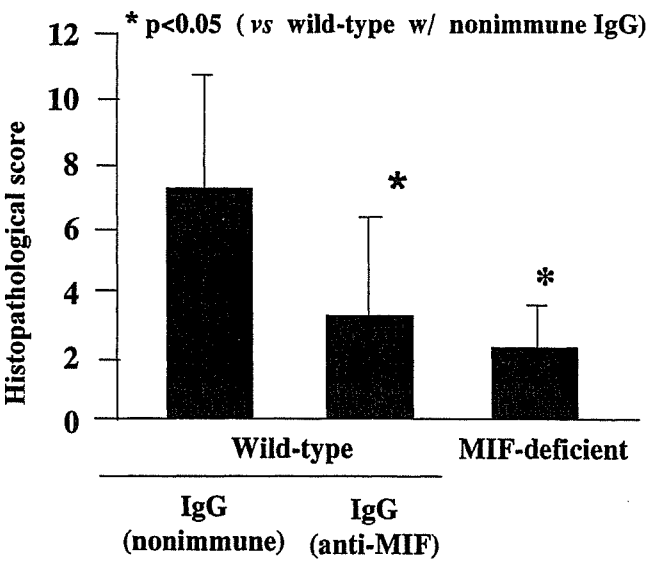

＊結果は文献３） ４）より引用

考察

1. MIF がチロシンキナーゼ、PKC、および転写調節因子 AP-1、NF-κB の活性化を介して滑膜繊維芽細胞の IL-8 転写を誘導すること、この誘導メカニズムは IL-1β のそれと共通し、かつ内因性 IL-1 の産生を介さないことが明らかとなった。滑膜細胞の産生する IL-8 は RA において好中球の動因に非常に重要であり、好中球はフリーラジカルやプロテアーゼにより軟骨破壊を行う。従来 MIF の RA における軟骨破壊機序がいくつか提唱されてきたが、本研究により MIF がこれに関与する新たな機序が推測された。

2. 1 の知見は、実験的関節炎を用いた in-vivo の検討でも確認された。関節炎の発症に伴い MIF は early-responsive に発現し、滑膜細胞に autocrine に作用して MMP-13 による軟骨破壊や、MIP-2 によって誘導される好中球浸潤に伴う軟骨破壊をコントロールしていると思われる（図 5）。

図 5

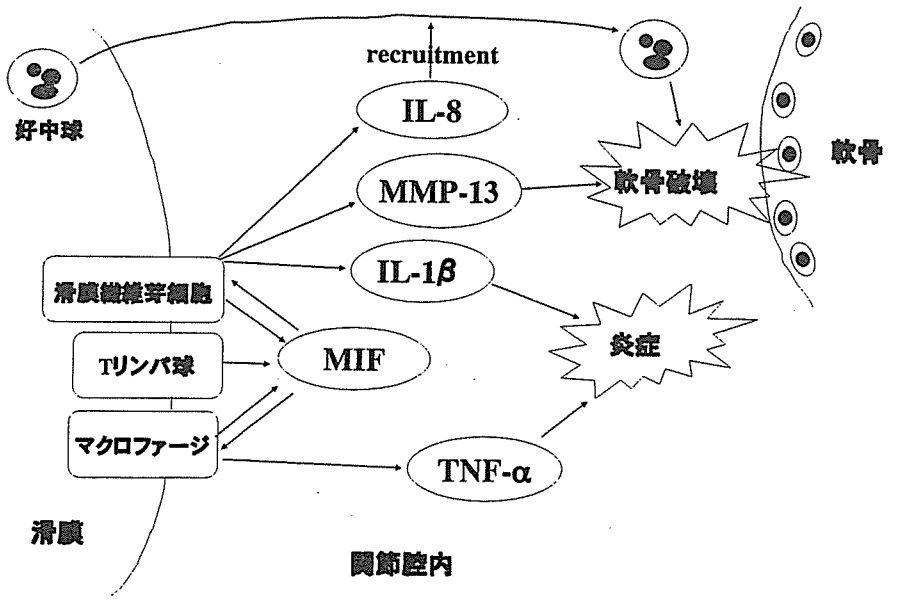

謝辞

本研究の共同研究者は、北海道大学大学院医学研究科分子医科学分野の西平順および北海道大学大学院分子生物学分野の小山芳一である。また、本研究を援助していただきました大和証券ヘルス財団研究助成に深謝申し上げます。

文献

1) Onodera, S., Tanji, H., Suzuki, K., Kaneda, K., Mizue, Y., Sagawa, A., & Nishihira, J. : High expression of macrophage migration inhibitory factor in the synovial tissues of rheumatoid joints. Cytokine, 11 : 163-167, 1999.

2) Onodera, S., Kaneda, K., Mizue, Y., Koyama, Y., Fujinaga, M., & Nishihira, J. : Macrophage Migration Inhibitory Factor (MIF) Up-regulates Expression of Matrix Metalloproteinases in Synovial Fibroblasts of Rheumatoid Arthritis. J. Biol. Chem., 275 : 444-450, 2000.

3) Onodera, S., Nishihira, J., Koyama, Y., Majima, T., Aoki, Y., Ichiyama, H., Ishibashi, T., & Minami, A. : Macrophage Migration Inhibitory Factor (MIF) Up-regulates Expression of Interleukin (IL)-8 mRNA in Synovial Fibroblasts of Rheumatoid Arthritis; Common Transcriptional Regulatory Mechanism between IL-8 and IL-1β . Arthritis Rheum, May;50(5):1437-47, 2004.

4) Ichiyama, H., Onodera, S., Nishihira, J., Ishibashi, T., Nakayama, T., Minami, A., Yasuda, K., & Tohyama, H. : Inhibition of Joint Inflammation and Destruction Induced by Anti-type II Collagen Antibody/Lipopolysaccharide (LPS)-induced Arthritis in Mice due to Deletion of Macrophage Migration Inhibitory Factor (MIF). Cytokine, 26(5):187-94, 2004.

Artificial Organs
28(11):1050–1054, Blackwell Publishing, Inc.

Thoughts and Progress

Relation Between Vertical Orientation and Stability of Acetabular Component in the Dysplastic Hip Simulated by Nonlinear Three-dimensional Finite Element Method

Hisashi Oki, Masao Ando, Hironori Omori, Yasuhiro Okumura, Kohei Negoro, Kenzo Uchida, and Hisatoshi Baba
Department of Orthopaedic Surgery, Faculty of Medicine, University of Fukui, Matsuoka, Fukui, Japan

Abstract: In acetabular dysplasia, more vertical orientation of the acetabular component is often used to minimize the superolateral bone grafting. This study was designed to determine the effects of vertical orientation of the cup on the stability and polyethylene wear of the acetabular component in uncemented total hip arthroplasty (THA). Three-dimensional finite element models of the hemipelvis with dysplastic acetabulum were developed. Metal-backed hemispherical cups were placed in the true acetabulum with abduction angles of 35, 45, 55, and 65 degrees. It was found that more vertical orientation of the cup was associated with larger relative motion of the metal shell between the acetabulum and metal shell. Furthermore, tilting and torsional shear stresses in the model of the cup abduction angle of 65 degrees were found to be 1.7 times larger than that in the model with 35 degrees at the bone–metal shell interface. More vertically oriented cups caused larger contact stresses at the articulating surfaces of the polyethylene liners. The results suggest that the abduction angle of the acetabular component significantly influences cup loosening and polyethylene wear in THA. **Key Words:** Cup abduction angle—Acetabular component—Relative motion—Shear stress—Contact stress.

In congenital dysplastic hips, uncemented fixation of the acetabular component may be associated with certain complications. Bony defect in the superolateral portion of the acetabulum is frequently encountered during total hip arthroplasty (THA). In many cases with dysplastic hips, the acetabular components need to be covered with bone grafts. Resorption of the bulky autografts is a major problem at long-term follow-up (1,2). In smaller grafts, resorption is not a significant feature (3). Several methods have been proposed to minimize the bone grafting, including the use of a special implant (4), more vertical orientation of the cup (5), medialization of the cup (6), and higher positioning of the cup relative to the true acetabulum (7–9). Controversy continues regarding the best method of treatment.

Although more vertical orientation of the cup can reduce the size of the bone graft, several studies have shown that more vertical orientation of the cup correlates with increased risks of cup loosening (5,10) and polyethylene wear (11–13). Several reports, however, showed no relationship between the cup abduction angle and polyethylene wear (14,15).

Ito et al. (16) showed that vertical migration and increase in vertical rotation tend to occur in acetabular components using bone grafting during early period after hybrid THA.

The purpose of this study was to investigate the effect of varying cup abduction angles in uncemented THA using nonlinear three-dimensional (3-D) finite element (FE) method on relative motion between the acetabulum and the metal shell, shear stress at the bone–metal shell interface, and contact stress at the articulating surface.

MATERIALS AND METHODS

Three-dimensional FE models were developed based on CT scan data of the right female hemipelvis with dysplastic acetabulum. Metal-backed hemispherical cups with 48 mm outer diameter were placed in the true acetabulum at abduction angles of 35, 45, 55, or 65 degrees. In the models with cup abduction angles of 35, 45, and 55 degrees, some elements were added to simulate superolateral cancellous bone grafting (Fig. 1). These cups had a polyethylene liner without elevated rim. These acetabular components articulated with 22.225 mm cobalt–chromium ball head with 0.05 mm radial clearance between the head and inner surface of the polyethylene liner.

The head consisted of 120 eight- and six-node elements and 173 nodes. The polyethylene liner consisted of 96 eight-node elements and 147 nodes. The metal shell consisted of 48 eight-node elements and 98 nodes. The polyethylene liner had two layers and the metal shell had a single 3-mm thick layer. The pelvic bone consisted of 6506 four-node elements and

Received February 2004; revised May 2004.
Address correspondence and reprint requests to Dr. Hisashi Oki, Department of Orthopaedic Surgery, Faculty of Medicine, University of Fukui, Shimoaizuki 23, Matsuoka, Fukui 910-1193, Japan. E-mail: SEIKEI68@fmsrsa.fukui-med.ac.jp

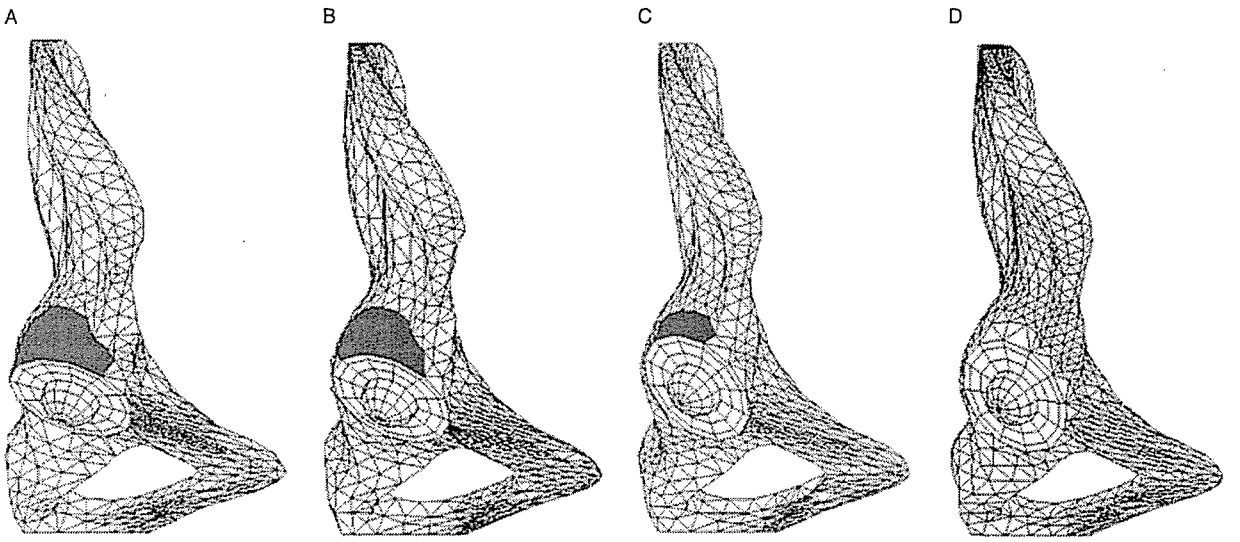

FIG. 1. Anterolateral views of the three-dimensional finite element models. Metal-backed hemispherical cups were placed in the true acetabulum with abduction angles of 35 (A), 45 (B), 55 (C), and 65 degrees (D). In the models with cup abduction angles of 35 (A), 45 (B), and 55 degrees (C) some elements were added to simulate superolateral cancellous bone graft (the bone graft is painted gray).

1780 nodes. The graft bone with cup abduction angle of 35 degrees consisted of 141 four-node elements and 68 nodes; the graft bone with cup abduction angle of 45 degrees consisted of 57 four-node elements and 36 nodes; and the graft bone with cup abduction angle of 55 degrees consisted of 21 four-node elements and 21 nodes. The elements of the pelvic bone and graft bone were constructed automatically.

Coefficients of friction, determined for earlier studies, were included at the interfaces between the head and polyethylene liner ($\mu = 0.065$) (17), and between the bone and the metal shell ($\mu = 0.61$) (18). The interface between the graft bone and the pelvic bone was considered to be fully bonded, simulating only the situation that the graft bone was firmly fixed to the host bone. The interface between the metal shell and polyethylene liner was also fully bonded.

Material properties, elastic modulus, and Poisson's ratio were based on the values reported in previous studies (19,20).

The hip joint reaction force was applied to the center of the ball head. Its direction and magnitude during the single-stance phase of normal gait were based on the data of Keaveny and Bartel (21). The pelvic models were assumed to have fixed support at the sacroiliac joint and the pubic symphysis.

We calculated the relative motion between the acetabulum and the metal shell on the medial, lateral, anterior, and posterior portions. Furthermore, we evaluated the tilting and torsional shear stresses at the bone–metal shell interface (19) and the contact stress at the articulating surface of the polyethylene liner. These analyses were performed by using a commercial FE package (ADINA, ADINA-IN and ADINA-PLOT, Adina Engineering, Watertown, MA, U.S.A.) (22).

RESULTS

The maximum relative motions of the metal shell among the four nodal points correlated with the cup abduction angle (Fig. 2). Increasing the cup abduction angle from 35 to 65 degrees resulted in an increase of the maximum relative motion between the acetabulum and the metal shell from 65.7 to 96.9 μm. The lateral portion showed the largest relative motion in each model, suggesting that the acetabular component changed in valgus position under loading.

On the more vertical orientation of the cup, we found that the maximum tilting shear stress at the bone–metal shell interface was increased (Fig. 3). Increasing the cup abduction angle from 35 to 65 degrees resulted in an increase of the maximum tilting shear stress at the bone–metal shell interface from 9.7 to 16.9 MPa. The maximum torsional shear stress at that interface showed similar change to the maximum tilting shear stress (9.7–17.0 MPa) (Fig. 3).

In more vertically oriented cups, the maximum contact stress at the articulating surface of polyethylene liner was enlarged (Fig. 4). Increasing the cup

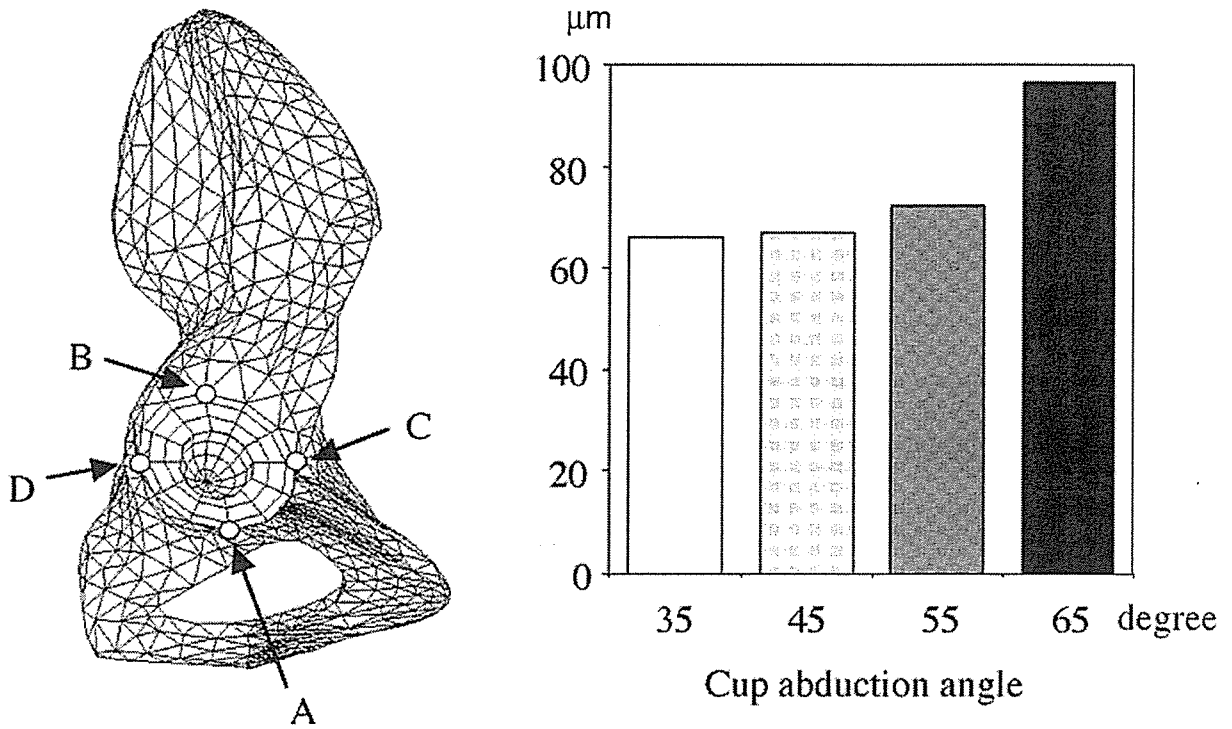

FIG. 2. The maximum relative motions between the acetabulum and the metal shell in each model. The value is the maximum relative motion among the medial (A), lateral (B), anterior (C), and posterior (D) nodal points on the outer surface of the metal shell.

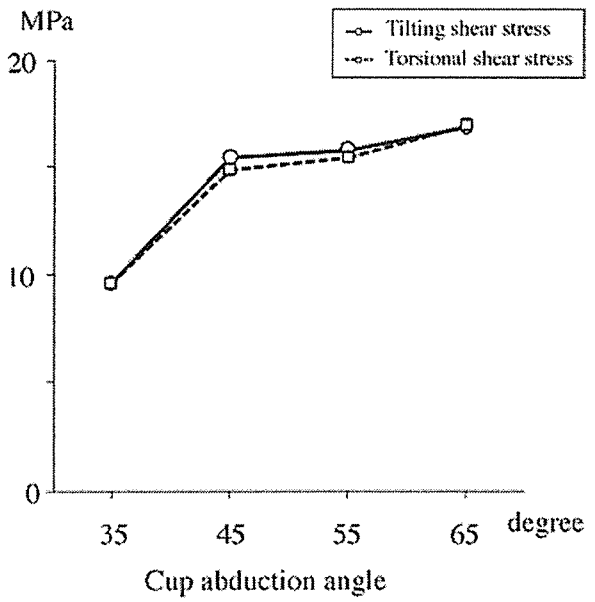

FIG. 3. The maximum tilting and torsional shear stresses at the bone–metal shell interface in each model.

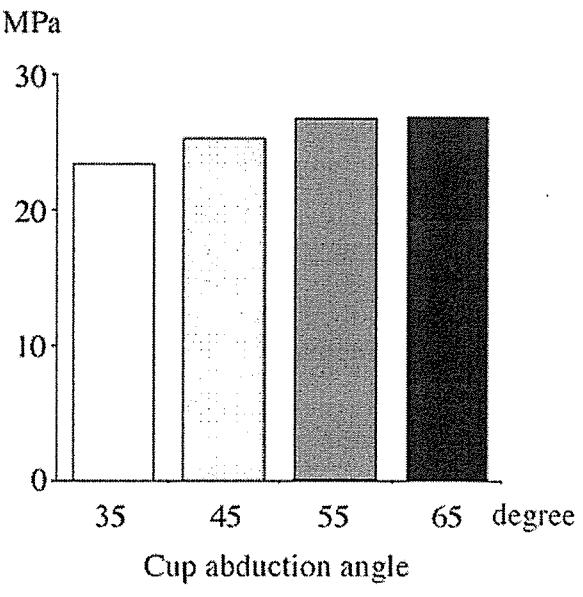

FIG. 4. The maximum contact stresses at the articulating surface in each model.

angle from 35 to 65 degrees was associated with increased maximum contact stress at the articulating surface from 23.4 to 26.8 MPa.

DISCUSSION

In clinical cases, vertical migration of loosening cup with bone grafting is often encountered. Our results suggest that all our models of the acetabular component tended to move to valgus position under loading in the simulation of the initial stability.

The development of press-fit prostheses is dependent on initial stability for promotion of bony ingrowth. To achieve bony ingrowth, relative motion between the implants and the surrounding bone should be minimized (23–27). Engh et al. (28) demonstrated that bony ingrowth could occur in the presence of relative motion <40 μm and implants could be well fixed, while excess relative motion of ≥150 μm results in stabilization of implant by fibrous tissue.

In a 3-D FE study (29), debonding of the stem–cement interface in THA was found to precede clinical failure of femoral components. This debonding was governed by the shear stress at the interface between components. Others demonstrated using FE analysis that tilting shear stress at the cement–bone interface was up to threefold greater in cases with severe dysplasia than in those with mild dysplasia (19). In uncemented model, the interface is stressed as the shear stress is related to the probability of mechanical failure and interface disruption (30).

Previous studies showed that the wear and failure of polyethylene surface contribute to long-term problems of the acetabular component. The polyethylene wear debris can cause osteolysis and loosening of implants (31,32). Other studies reported that contact stress at the articulating surface is associated with surface damage of the polyethylene liner (13,33–35), although the precise mechanism relating contact stress to wear debris remains unclear.

A number of investigators have demonstrated that the cup abduction angle correlates with cup loosening and polyethylene wear, clinically or biomechanically. Knight and Fujii (1993) used radiography to identify the factors that affect cup loosening in patients with bone grafting during THA. They concluded that acetabular component loosening was associated with initial cup abduction angle of ≥50 degrees. With 3-D radiographic examination of polyethylene wear, Devane and Horne (1997) reported a significantly greater volumetric wear rate in patients with vertically oriented acetabular cup. Other groups (14,15), however, reported that polyethylene wear did not significantly increase with widening of the cup abduction angle, based on radiographic examination. Furthermore, Kurtz and Edidin (1997) investigated the effects of cup orientation on contact stress associated with surface damage in polyethylene liner by using 3-D FE methods. They showed that the contact stress at the articulating surface of vertically oriented acetabular cup was larger than that of horizontally oriented one.

The results of this study suggested that more vertical orientation of the uncemented acetabular component caused larger relative motion between the bone and the metal shell, larger shear stress at the bone–metal shell interface, and larger contact stress at the articulating surface of the polyethylene liner. Thus, more vertical orientation of the cup was associated with cup loosening and polyethylene wear. We conclude that the cup abduction angle significantly influences cup loosening and wear generation in THA.

Acknowledgment: This work was supported in part by a Grant-in-Aid for General Scientific Research of the Ministry of Education, Science and Culture of Japan (grant no. 09470311).

REFERENCES

1. Shinar AA, Harris WH. Bulk structural autogenous grafts and allografts for reconstruction of the acetabulum in total hip arthroplasty. Sixteen-year-average follow-up. *J Bone Joint Surg Am* 1997;79-A:159–68.
2. Mulroy RD Jr, Harris WH. Failure of acetabular autogenous grafts in total hip arthroplasty. Increasing incidence: a follow-up note. *J Bone Joint Surg Am* 1990;72-A:1536–40.
3. Wolfgang GL. Femoral head autografting with total hip arthroplasty for lateral acetabular dysplasia. A 12-year experience. *Clin Orthop* 1990;255:173–85.
4. Köster G, Willert HG, Köhler HP, Döpkens K. An oblong revision cup for large acetabular defects: design rationale and two- to seven-year follow-up. *J Arthroplasty* 1998;13: 559–69.
5. Kennedy JG, Rogers WB, Soffe KE, Sullivan RJ, Griffen DG, Sheehan LJ. Effect of acetabular component orientation on recurrent dislocation, pelvic osteolysis, polyethylene wear, and component migration. *J Arthroplasty* 1998;13:530–4.
6. Dunn HK, Hess WE. Total hip reconstruction in chronically dislocated hips. *J Bone Joint Surg Am* 1976;58-A:838–45.
7. Kelley SS. High hip center in revision arthroplasty. *J Arthroplasty* 1994;9:503–10.
8. Pagnano W, Hanssen AD, Lewallen DG, Shaughnessy WJ. The effect of superior placement of the acetabular component on the rate of loosening after total hip arthroplasty. *J Bone Joint Surg Am* 1996;78-A:1004–14.
9. Russotti GM, Harris WH. Proximal placement of the acetabular component in total hip arthroplasty. A long-term follow-up study. *J Bone Joint Surg Am* 1991;73-A:587–92.
10. Knight JL, Fujii K, Atwater R, Grothaus L. Bone grafting for acetabular deficiency during primary and revision total hip arthroplasty. A radiographic and clinical analysis. *J Arthroplasty* 1993;8:371–82.
11. Bono JV, Sanford L, Toussaint JT. Severe polyethylene wear in total hip arthroplasty. Observations from retrieved AML

PLUS hip implants with an ACS polyethylene liner [see comments]. *J Arthroplasty* 1994;9:119–25.
12. Devane PA, Horne JG, Martin K, Coldham G, Krause B. Three-dimensional polyethylene wear of a press-fit titanium prosthesis. Factors influencing generation of polyethylene debris. *J Arthroplasty* 1997;12:256–66.
13. Kurtz SM, Edidin AA, Bartel DL. The role of backside polishing, cup angle, and polyethylene thickness on the contact stresses in metal-backed acetabular components. *J Biomech* 1997;30:639–42.
14. Del Schutte H Jr, Lipman AJ, Bannar SM, Livermore JT, Ilstrup D, Morrey BF. Effects of acetabular abduction on cup wear rates in total hip arthroplasty. *J Arthroplasty* 1998;13: 621–6.
15. Woolson ST, Murphy MG. Wear of the polyethylene of Harris–Galante acetabular components inserted without cement. *J Bone Joint Surg Am* 1995;77-A:1311–4.
16. Ito H, Matsuno T, Minami A, Aoki Y. Intermediate-term results after hybrid total hip arthroplasty for the treatment of dysplastic hips. *J Bone Joint Surg Am* 2003;85-A:1725–32.
17. Lu Z, McKellop H. Frictional heating of bearing materials tested in a hip joint wear simulator. *Proc Inst Mech Eng [H]* 1997;211:101–8.
18. Shirazi-Adl A, Dammak M, Paiement G. Experimental determination of friction characteristics at the trabecular bone/ porous-coated metal interface in cementless implants. *J Biomed Mater Res* 1993;27:167–75.
19. Schüller HM, Dalstra M, Huiskes R, Marti RK. Total hip reconstruction in acetabular dysplasia. A finite element study. *J Bone Joint Surg Br* 1993;75-B:468–74.
20. Dalstra M, Huiskes R. Load transfer across the pelvic bone. *J Biomech* 1995;28:715–24.
21. Keaveny TM, Bartel DL. Effects of porous coating, with and without collar support, on early relative motion for a cementless hip prosthesis. *J Biomech* 1993;26:1355–68.
22. Harrigan TP, Harris WH. A finite element study of the effect of diametral interface gaps on the contact areas and pressures in uncemented cylindrical femoral total hip components. *J Biomech* 1991;24:87–91.
23. Cameron HU, Pilliar RM, MacNab I. The effect of movement on the bonding of porous metal to bone. *J Biomed Mater Res* 1973;7:301–11.
24. Cook SD, Thomas KA, Haddad RJ Jr. Histologic analysis of retrieved human porous-coated total joint components. *Clin Orthop* 1988;234:90–101.
25. Heck DA, Nakajima I, Kelly PJ, Chao EY. The effect of load alteration on the biological and biomechanical performance of a titanium fiber–metal segmental prosthesis. *J Bone Joint Surg Am* 1986;68-A:118–26.
26. Pilliar RM, Lee JM, Maniatopoulos C. Observations on the effect of movement on bone ingrowth into porous-surfaced implants. *Clin Orthop* 1986;208:108–13.
27. Soballe K, Hansen ES, B-Rasmussen H, Jorgensen PH, Bunger C. Tissue ingrowth into titanium and hydroxyapatite-coated implants during stable and unstable mechanical conditions. *J Orthop Res* 1992;10:285–99.
28. Engh CA, O'Connor D, Jasty M, McGovern TF, Bobyn JD, Harris WH. Quantification of implant micromotion, strain shielding, and bone resorption with porous-coated anatomic medullary locking femoral prostheses. *Clin Orthop* 1992;285: 13–29.
29. Verdonschot N, Huiskes R. Cement debonding process of total hip arthroplasty stems. *Clin Orthop* 1997;336:297–307.
30. Huiskes R, van Rietbergen B. Preclinical testing of total hip stems. The effects of coating placement. *Clin Orthop* 1995; 319:64–76.
31. Harris WH. Osteolysis and particle disease in hip replacement. A review. *Acta Orthop Scand* 1994;65:113–23.
32. Howie DW, Vernon RB, Oakeshott R, Manthey B. A rat model of resorption of bone at the cement–bone interface in the presence of polyethylene wear particles. *J Bone Joint Surg Am* 1988;70-A:257–63.
33. Bartel DL, Burstein AH, Toda MD, Edwards DL. The effect of conformity and plastic thickness on contact stresses in metal-backed plastic implants. *J Biomech Eng* 1985;107:193–9.
34. Bartel DL, Bicknell VL, Wright TM. The effect of conformity, thickness, and material on stresses in ultra-high molecular weight components for total joint replacement. *J Bone Joint Surg Am* 1986;68-A:1041–51.
35. Jin ZM, Dowson D, Fisher J. A parametric analysis of the contact stress in ultra-high molecular weight polyethylene acetabular cups. *Med Eng Phys* 1994;16:398–405.

Artificial Organs
29(5):387–392, Blackwell Publishing, Inc.

Dynamic Analysis of the Resultant Force Acting on the Hip Joint During Level Walking

Naoki Hashimoto, Masao Ando, Takafumi Yayama, Kenzo Uchida, Shigeru Kobayashi, Kohei Negoro, and Hisatoshi Baba

Division of Orthopaedics and Rehabilitation Medicine, Department of Surgery, University of Fukui Faculty of Medicine, Matsuoka, Fukui, Japan

Abstract: The present study was designed to determine the resultant force acting on the hip joint during walking using a new dynamic analysis method. Our model utilized joint motion, ground reaction force, and muscle strength data from 18 women (6 normal women aged 20–24 years, 6 normal women aged 50–57 years, and 6 female patients with osteoarthritis, aged 50–66 years). We analyzed the resultant force using the multibody dynamic analysis system. To determine the factors that influence the force acting on the hip, we examined the effect of age and total hip arthroplasty. The maximum resultant force acting on the femoral head was dependent on the subject body weight and correlated with muscle strength and walking speed. The results of this study highlight the agreement between computer simulation analysis and actual measurement of the resultant force acting on the hip. Our results suggest that muscle strength and walking speed are significant determinants of the resultant force acting on the hip. **Key Words:** Hip joint—Mathematical model—Resultant force—Electromyography—Total hip arthroplasty.

Total hip arthroplasty (THA) is a widely used method for treatment of patients with degenerative hip osteoarthritis (OA). It is well recognized that long-term stability of THA is significantly affected by wear of the implants and the quality of the implanted materials (1–3). In addition, even in patients who undergo THA with a uniform surgical technique, the magnitude of wear of the implants and biomechanical stability vary considerably and thus the longevity of THA is the most difficult issue to be considered (4,5). To predict the fate of individual THA, biomechanical simulation (6,7) and load analysis to test the stability of the implants and mechanical tests (8) have been advocated. However, it is essential to consider and analyze the resultant force acting on the hip joint under walking conditions. Several investigators have analyzed the resultant force in an individual candidate, but the magnitude and direction of the force are still major unknown issues (9–14). At present, the best method for investigating the load force is the in vivo analysis through built-in telemetric sensors in THA patients (12–15), but this method is difficult for serial analysis of the force or at an arbitrary point in each patient.

In the present study, to analyze the resultant force acting on the individual hip joint before and after THA, we used a three-dimensional computer simulation based on gait analysis data and electromyographic (EMG) data. We also investigated the influence on the force of age of the subject, the walking speed, and surgical intervention.

SUBJECTS

Table 1 lists the mean age, height, and weight of the 18 subjects who participated in the study. The subjects comprised 6 healthy women aged 20–24 years, 6 healthy women aged 50–57 years, and 6 female patients with unilateral OA of the hip joint, without any physical handicap, aged 50–66 years. In patients with unilateral OA of the hip joint, gait analysis was performed preoperatively and repeated at least 6 months after THA. We used cementless cup (AMS Cup, Japan Medical Materials, Osaka, Japan)

Received October 2004; revised December 2004.
Address correspondence and reprint requests to Dr. Naoki Hashimoto, Division of Orthopaedics and Rehabilitation Medicine, Department of Surgery, University of Fukui Faculty of Medicine, Shimoaizuki 23, Matsuoka, Fukui 910-1193, Japan. E-mail: nhassy@fmsrsa.fukui-med.ac.jp

TABLE 1. *Female subjects*

	Young normal group ($n = 6$)	Old normal group ($n = 6$)	Hip OA group ($n = 6$)
Age (year)	21.2 ± 1.6 (20–24)	53.1 ± 2.6 (50–57)	58.2 ± 5.5 (50–56)
Height (cm)	152.3 ± 6.3 (142.5–160.2)	150.3 ± 4.4 (147.0–158.5)	150.4 ± 7.0 (141.5–163.0)
Body weight (kg)	47.9 ± 5.5 (42.0–56.5)	52.3 ± 8 (44.5–62.5)	55.7 ± 9.4 (40.0–66.0)

Data are mean ± SEM and (range). OA, osteoarthritis.

and cementless stem (FMS-Anatomic Stem, Japan Medical Materials) with a 28-mm alumina head in all 6 patients. They had a successful clinical and radiographic outcome, and could walk without support such as canes. The study protocol was approved by the Human Ethics Review Committee of Faculty of Medicine, Fukui University, and a signed consent form was obtained from each subject.

PROTOCOL

We used two software programs to analyze the resultant force acting on the hip joint. The first one was the musculoskeletal modeling software (SIMM/Gait, MusculoGraphics, Chicago, IL, U.S.A.) (16), and the second was the multibody dynamic software package (ADAMS/Android and ADAMS/View version 9.04, Mechanical Dynamics, Ann Arbor, MI, U.S.A.) (17). SIMM/Gait can calculate muscle strength using the Hill type model from sequential changes in the joint angle and percentage maximum voluntary isometric contraction (% MVIC) (18) of each muscle. ADAMS/Android can create a rigid body model based on various physical attributes (e.g., body height, weight, and the length and circumference of each body section) automatically. ADAMS/View can also simulate dynamic analysis of the resultant forces acting on the hip joint by inserting sequential changes in the joint angle, muscle strength, and ground reaction force into the model.

A flow chart of this analysis is shown in Fig. 1. Reflective markers were mounted at 13 sites including the anterior superior iliac spine, sacrum, femoral center, lateral knee joint, center of the lower leg, lateral malleolus, and head of the third metatarsal. The subject was instructed to walk along an 8-m-long pedestrian passage of a 10-m-long walkway (Fig. 2). For the gait analysis, three conditions such as normal walking, fast walking, and slow walking were set without any restrictions. Angle changes on the frontal, horizontal, and sagittal surfaces were determined for the pelvis, hip joint, and foot joint by using a three-dimensional movement analysis apparatus (VICON 370, Oxford Metrics, Oxford, U.K.) equipped with 6 high-speed video cameras. The angles were calculated with reference to adjacent segment orientations. Ground reaction forces were recorded synchronously with the kinematic data using four force platforms (LG6-4 by AMTI, Watertown, MA, U.S.A.) located in the center of the 10-meter-long walkway. Muscle activities were recorded using electromyographic telemeters (TEL-EMG, BTS, Milan, Italy). We recorded the EMG of the muscles that were considered most important in walking rather than all muscles because it was not possible to record and analyze the electric activities of all lower limb muscles. The electrodes were placed over the gluteus maximus, gluteus medius, adductor longus, rectus femoris, and tensor of fascia lata. These measurements described above were automatically synchronized with the first heel contact on

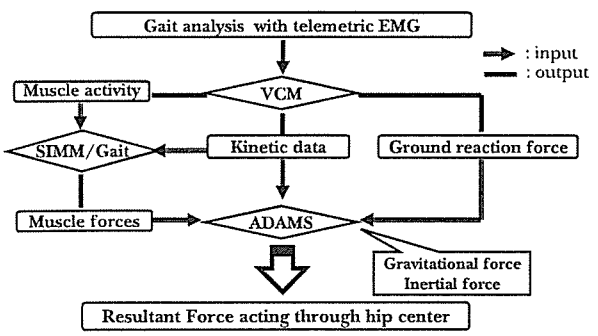

FIG. 1. Flow chart of the dynamic analysis of resultant force.

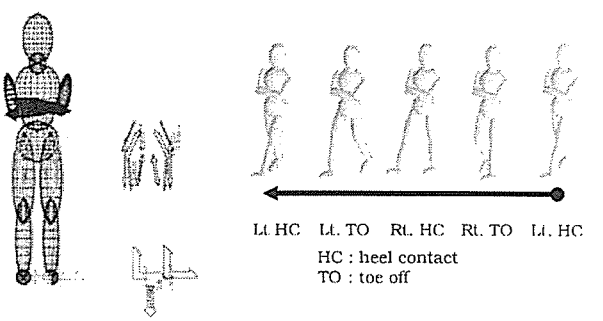

FIG. 2. Model for dynamic analysis of one gait cycle.

the device to record the ground reaction force as a trigger. We recorded these measurements 6 times for each of the 3 walking patterns (normal, fast, and slow walking patterns).

All data were fed into software for 3-dimensional analysis of actions (VCM, Oxford Metrics) in order to calculate the sequential changes in joint angle, sequential changes in the ground reaction force, cadence, walking speed, and EMG activity of each muscle. From the EMG activity during walking and at maximum muscle contraction by manual examination of the muscle activity obtained from the electromyographic telemeter, the percentage MVIC was computed and the muscle strength was estimated by using the SIMM/Gait software. The duration of the stride temporal phase was expressed as a percentage of the duration of a single gait cycle. All data (joint motion, ground reaction force, muscle strength) representing the time-course of different variables were normalized in time (the duration of the whole gait cycle was considered as 100 percent, divided in time to yield a normalized gait cycle of 50 phases (19,20)). A rigid body model was formed by the ADAMS/Android software. We calculated the changes in muscle strength during walking using SIMM/Gait, which calculates muscle strength using the Hill type model from changes in the main muscle based on joint motion and percentage MVIC recorded using the VCM (16,21). First, we transformed the raw muscle activity to percentage MVIC value among items set beforehand, generating each muscle strength in the property of the SIMM/gait software. Second, we fed the changes in three-dimensional joint angle in each of the hip, knee, ankle joints that occurred in a single gait cycle into the SIMM/gait software after excluding the activities of other muscles recorded from the gait analysis. Finally, we did simulation analysis and calculated the muscle strength in every phase. For the data from the VCM and SIMM/Gait installed in this model, we added 5 spring components that generated the above-mentioned muscle contraction force as internal forces in anatomical positions of the rigid body model. The center of the hip joint of a subject was selected from the anteroposterior and lateral views of the X-ray photograph. We also measured the distance from the hip joint center to the anatomic origin and insertion of each muscle. We plotted the origin and halt of spring model generating muscle strength on the coordinate, which assumed a hip joint center (0,0,0) in a rigid body model formed by the ADAMS/Android. We also attached a damper component of the external force, due to the contact between the foot and ground, which was obtained from the ground reaction force in the foot segment.

DATA PROCESSING AND ANALYSIS

The computer simulations for dynamic analysis of the resultant forces were generated using ADAMS/View. We did simulations for each joint in the simulation model that was generated as described above; the joint movement was generated from the sequential changes in the joint angle, the muscle strength generated by the spring model from SIMM data, and the ground reaction force was generated in the foot segment. For the analysis, each joint of the upper extremities was constrained, the pelvis kept stationary, and the angle of each joint of the lower extremities maintained in a symmetrical position. All data were converted to Akima spline functions. The friction in the joint, represented by hinges, is extremely small and can therefore be ignored. The local axes are orthogonal. For the transformation to the coordinate system, the local z axis (longitudinal axis) of the hip joint coordinate system was determined by a vector from the center of the femoral head to the pelvis. The local x axis (anteroposterior direction) was defined by drawing a line perpendicular to the local z axis. The local y axis (mediolateral) was defined by drawing a line perpendicular to the local z-axis (22). We calculated the components of the force in the x, y, and z directions; that is, Fx, Fy, and Fz. The square of the resultant force was defined as $|Fx|^2 + |Fy|^2 + |Fz|^2$. We output the direction of resultant force by plotting the numerical values of Fx, Fy, and Fz for every phase as a coordinate on the xy plane (horizontal plane), xz plane (sagittal plane), and yz plane (coronal plane). We examined the effects of the resultant force based on walking speed, age, and preoperative and postoperative walking status. We used several parameters (walking speed, cadence, and ratio of single stance phase and double stance phase, moment) for the analysis.

All data are expressed as mean ± SEM. Differences in the resultant force between paired data of the young normal group, old normal group, preoperative OA group and postoperative OA group were examined for statistical significance using the Student's t-test. The relationships between the resultant force and various gait parameters were examined by Pearson correlation analysis. A P value less than 0.05 denoted the presence of a statistically significant difference.

RESULTS

The wave pattern of the dynamic resultant force curve recorded in one gait cycle showed two peaks in both the normal group and OA group. The maximum force occurred at the first peak in the gait cycle.

TABLE 2. *Individual and mean resultant force of each subject and group (normal walking speed)*

Subjects	Young normal group	Old normal group	Osteoarthritis group	
			Preoperative	Postoperative
1	396.2	319.4	246.0	292.4
2	336.8	309.6	265.9	290.4
3	378.5	291.9	283.7	314.4
4	362.7	322.6	246.4	301.6
5	321.4	316.6	302.2	333.7
6	308.9	268.5	265.3	289.6
Mean ± SEM	350.7 ± 34.0	304.8 ± 20.9	268.3 ± 21.8	303.7 ± 17.4

The resultant force is expressed as % of body weight.

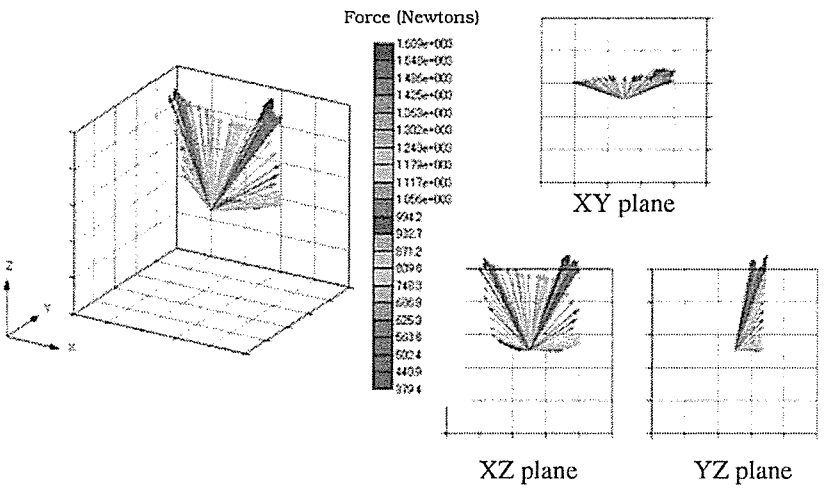

FIG. 3. Direction of resultant force acting on the hip. Analysis in a representative young normal subject (Subject 1).

The maximum value of the resultant force during normal walking speed, in both the normal group and OA group was about two or three times the body weight in most cases (Table 2). The direction of the maximum resultant force was anteromedial and posteromedial above the center of the femoral head (Fig. 3). The maximum resultant force increased by walking speed in the same subject when the speed was actively changed, and a steeper wave pattern was evident (Fig. 4). The resultant force changed significantly with walking speed, step length, and the single leg support period in the two different age groups (young normal group and old normal group). Significant differences were also noted in flexion, extension, and adduction moment with regard to muscle strength between the two age groups (young normal group and old normal group).

The anteroposterior direction force (Fx) and vertical direction force (Fz) of the old normal group were smaller than those of the young normal group. Similarly, the resultant force was significantly different between the two groups (young normal group and old normal group) (Fig. 5). The resultant force was significantly different between old normal group and preoperative of OA group but the resultant force was not significantly different between old normal group and postoperative of OA group. Walking speed, step, and single leg support period ratio improved postoperatively in the OA group compared with the respective preoperative values. Abduction moment also improved significantly postoperatively, and extension moment measured postoperatively was larger than the preoperative value. The postoperative resultant force, progress direction

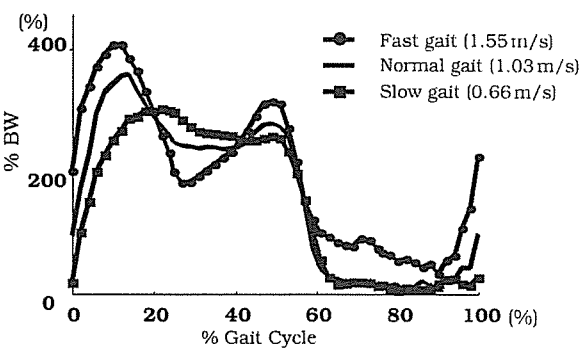

FIG. 4. Resultant force acting on the hip as a function of walking speed. Analysis of a representative young normal subject (Subject 1).

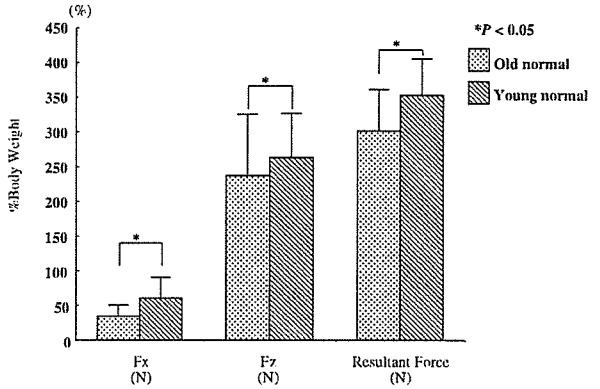

FIG. 5. Comparison of resultant force between young and old normal subjects at normal walking speed. Data are mean ± SEM.

component force (*Fx*), and plumb direction component force (*Fz*) showed significant improvement relative to the preoperative values (Fig. 6). The resultant force correlated significantly with muscle strength and also with various gait parameters including gait speed, stride, single stance phase, flexion moment, extension moment, abduction moment, and adduction moment (Table 3).

DISCUSSION

Studies that estimate the resultant forces acting on the hip joint during locomotion are generally divided into two groups: studies that use mathematical models (9–11) and those in which actual data are obtained from telemeters implanted into joint prostheses (12–14). Instrumented telemetric implant studies can provide the most accurate measurements and many activities, but such studies are difficult ethically, and have several problems (costly, technically complex, offer no direct benefit to the patients, and

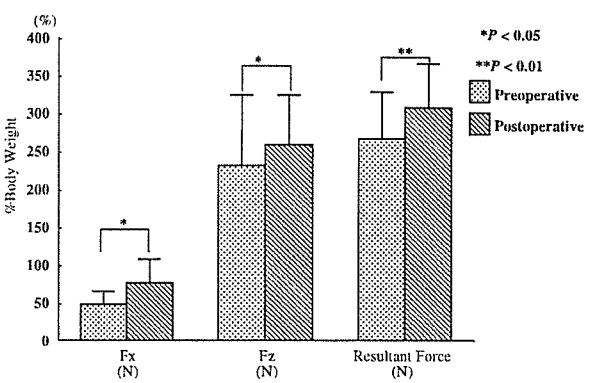

FIG. 6. Comparison of preoperative and postoperative resultant force in patients with OA (normal walking speed). Data are mean ± SEM.

TABLE 3. *Results of correlation analysis of resultant force and various gait parameters in patients with OA after total hip arthroplasty*

	Correlation coefficient	*P* value
Gait speed	0.801	<0.01
Stride	0.402	<0.01
Single stance phase	0.486	<0.05
Flexion moment	0.667	<0.01
Extension moment	0.731	<0.05
Abduction moment	0.675	<0.01
Adduction moment	0.413	<0.01

cannot study truly normal subjects). Accordingly, we used mathematical models in the present study. However the principal limitation of mathematical predictions lies in making one or more assumptions, which should be validated. Interestingly, the results of previous reports in the literature suggest that the predicted hip resultant force is consistently higher than direct-force measurements, although both the predictions and measurements exhibit reasonable internal consistencies (9–15).

By employing mathematical models, the resultant force was reported to be 330–500% body weight (BW) according to Crowninshield and Brand (9), 410–690% BW by Rohrle et al. (10), and 190–260% BW by Komistek et al. (11). In our study, the force was 250–360% BW. The resultant force measured directly by telemetry was reported at 260–280% BW by Davy et al. (12), 280% BW by Bergmann et al. (13), and 260% BW by Kotzor et al. (14). Brand et al. (15) stated that the analytical data obtained from mathematical models tend to be over a wider range and generally higher than the measured values and few approximate the actual data. On the other hand, the analytical data obtained in the present study for the resultant force were comparable with the actual figures. The curve lines were similar in that they showed a double-peak pattern with spikes on the first peak. However, the analytical data from the present study on the directions on both the sagittal and frontal planes generally agreed with those reported by Bergmann et al. (13) (those exceeding 75% of the maximum resultant force).

With regard to the relationship between walking speed and resultant force, Bergmann et al. (13) reported that the resultant force increased when walking speed increased in the experiment that used a telemeter type artificial joint in an in vivo study. These results were confirmed by Komistek et al. (11) who used a mathematical model. The results of the in vivo telemetry study by Crowninshield et al. (23) showed that the resultant force was influenced by muscle strength and walking

speed. Our results confirmed the findings of these earlier studies.

The resultant force acting on the hip joint increased in most subjects with the recovery of muscle strength and increased walking speed postoperatively. We think that various morphological changes (anteversion angle, femoral offset, neck shaft angle, leg length discrepancy) after THA have a great effect on improvement of muscle strength. We considered this problem in each subject by changing the plotting origin and halt of spring model that generates the muscle strength in a rigid body model. The Newtonian model of the lower extremity is designed to estimate the intersegmental resultant forces. Application of this model required maneuvering the hip center into the natural position during surgery, which reduced the resultant force acting on the hip joint (24). On the other hand, Kotzlar et al. (14) reported increase in the resultant force on the hip joint after operation. Among the impairments reported in the present study, the hip extensor moment decreased compared with the preoperative value in patients with OA (25). The decrease in the hip extensor moment correlated with walking speed. THA resulted in restoration of the muscle strength and increase in walking speed. Our results suggest that the resultant force acting on the hip joint increases as walking speed increases. Our conclusion in this study is that prediction by computer simulation depends on making some assumptions, and that the latter cannot be applied to all cases. For example, we think it is difficult to provide accurate simulation in certain patients such as those with severe developmental dislocation of the hip, deformed large femoral head of Perthes disease, and severe leg length discrepancy. However, our study emphasizes the importance of analysis of the resultant force on the hip joint for prediction of the durability of THA implant. To assess the hip joint force during daily life would help to solve these problems.

Acknowledgments: This study was supported by the Japanese Government Basic Research Grant (B) no. 09470311 of the Science Research Fund by the Ministry of Education, Culture, Sports, Science and Technology.

REFERENCES

1. Adler E, Stuchin SA, Kummer FJ. Stability of press-fit acetabular cups. *J Arthroplasty* 1992;7:295–301.
2. Dorr LD, Wan Z, Cohen J. Hemispheric titanium porous coated acetabular component without screw fixation. *Clin Orthop* 1998;351:158–68.
3. Kaper BP, Bernini PM. Failure of a constrained acetabular prosthesis of a total hip arthroplasty. A report of four cases. *J Bone Joint Surg Am* 1998;80-A:561–5.
4. Thomas BJ, Saa J, Lane JM. Total hip arthroplasty. *Curr Opin Rheumatol* 1996;8:148–53.
5. Kobayashi S, Eftekhar NS, Terayama K, Joshi RP. Comparative study of total hip arthroplasty between younger and older patients. *Clin Orthop* 1997;339:140–51.
6. Lu Z, McKellop H, Liao P, Benya P. Potential thermal artifacts in hip joint wear simulators. *J Biomed Mater Res* 1999; 48:458–64.
7. McKellop H, Shen FW, DiMaio W, Lancaster JG. Wear of gamma-crosslinked polyethylene acetabular cups against roughened femoral balls. *Clin Orthop* 1999;369:73–82.
8. Dujardin FH, Mollard R, Toupin JM, Coblentz A, Thomine JM. Micromotion, fit, and fill of custom made femoral stems designed with an automated process. *Clin Orthop* 1996;325: 276–89.
9. Crowninshield RD, Brand RA. A physiologically based criterion of muscle force prediction in locomotion. *J Biomech* 1981;14:793–801.
10. Rohrle H, Scholten R, Sigolotto C, Sollbach W, Kellner H. Joint forces in the human pelvis-leg skeleton during walking. *J Biomech* 1984;17:409–24.
11. Komistek RD, Stiehl JB, Dennis DA, Paxson RD, Soutas-Little RW. Mathematical model of the lower extremity joint reaction forces using Kane's method of dynamics. *J Biomech* 1998;31:185–9.
12. Davy DT, Kotzar GM, Brown RH, et al. Telemetric force measurements across the hip after total arthroplasty. *J Bone Joint Surg Am* 1988;70-A:45–50.
13. Bergmann G, Graichen F, Rohlmann A. Hip joint loading during walking and running measured in two patients. *J Biomech* 1993;26:969–90.
14. Kotzar GM, Davy DT, Berilla J, Goldberg VM. Torsional loads in the early postoperative period following total hip replacement. *J Orthop Res* 1995;13:945–55.
15. Brand RA, Pedersen DR, Davy DT, Kotzar GM, Heiple KG, Goldberg VM. Comparison of hip force calculations and measurements in the same patient. *J Arthroplasty* 1994;9:45–51.
16. Delp SL, Loan JP. A graphics-based software system to develop and analyze models of musculoskeletal structures. *Comput Biol Med* 1995;25:21–34.
17. Crupi V, La Rosa G. Kinematic and dynamic analysis of running under conditions of variable gravity. *Biomed Mater Eng* 1999;9:285–96.
18. Neumann DA, Cook TM. Effect of load and carrying position on the electromyographic activity of the gluteus medius muscle during walking. *Phys Ther* 1985;65:305–11.
19. Kadaba MP, Remakrishnan HK, Wooten ME. Measurement of lower extremity kinematics during level walking. *J Orth Res* 1990;8:383–92.
20. Romano CL, Frigo C, Randelli G, Pedotti A. Analysis of the gait of adults who had residua of congenital dysplasia of the hip. *J Bone Joint Surg Am* 1996;78-A:1468–79.
21. Riley PO, Kerrigan DC. Torque action of two-joint muscles in the swing period of stiff-legged gait: a forward dynamic model analysis. *J Biomech* 1998;31:835–40.
22. Hurwitz DE, Foucher KC, Sumner DR, Andriacchi TP, Rosenbrg AG, Galante JO. Hip motion and moments during gait relate directly to proximal femoral bone mineral density in patients with hip osteoarthritis. *J Biomech* 1998;31:919–25.
23. Crowninshield RD, Johnston RC, Andrews JG, Brand RA. A biomechanical investigation of the human hip. *J Biomech* 1978;11:75–85.
24. Johnston RC, Brand RA, Crowninshield RD. Reconstruction of the hip. A mathematical approach to determine optimum geometric relationships. *J Bone Joint Surg Am* 1979;61:639–52.
25. Perron M, Malouin F, Moffet H, McFadyen BJ. Three-dimensional gait analysis in women with a total hip arthroplasty. *Clin Biomech* 2000;15:504–15.

当科における関節リウマチに対する工藤式 type 5 人工肘関節置換術の治療成績

藤本理代　加藤博之*　岩崎倫政　三浪明男　三浪三千男**

Key Words : Rheumatoid arthritis（慢性関節リウマチ），Kudo elbow（工藤式人工肘関節），
Total elbow arthroplasty（人工肘関節置換術）

【目的】RA による肘関節障害に対する Kudo Elbow Type 5 人工肘関節置換術の治療成績を検討した．

【方法】対象は 1994 年以降，Kudo Elbow Type 5 を使用し，手術を施行した 52 肘のうち，2 年以上経過観察し得た 20 例・25 肘，男性 3 例・女性 17 例，手術時年齢は平均 61 歳であった．Larsen 分類では stageIV:18 肘，stage: V は 7 肘であった．手術手技は Kudo の方法 [2]に準じ Campbell の後方アプローチにて進入，尺骨神経は皮下前方移行を行った．後療法は術後 2 週間肘関節 70° 屈曲位でのシーネ固定を行い，術後 4 週間は夜間シーネ固定とした．上腕骨コンポーネントはセメント固定 2 肘・セメントレス固定 23 肘であった．尺骨コンポーネントは metal back type・セメント固定 6 肘，metal back type・セメントレス固定 3 肘，残りの 16 肘は all HDP type・セメント固定とした．経過観察期間は平均 4 年 11 ヵ月であった．臨床評価は，ROM・Mayo Elbow Performance Score [3]を用いた．X 線学的評価では各コンポーネントの上腕骨・尺骨に対する人工関節の設置角度・clear zone と loosening の有無について検討した．Clear zone はコンポーネントおよびセメント周囲の 2 ㎜以下の radiolucent line とし，2 ㎜より幅広い radiolucent line の存在や明らかなコンポーネントの転位は loosening と判定した．また術中・術後の合併症の有無についても調査した．

【結果】肘関節平均 ROM は，伸展は術前後とも–35° と伸展制限が残存したが，屈曲は術前 103° から 134°，回内は 52° から 65°，回外は 60° から 73° と改善された（図 1）．Mayo Score は 20 例で調査可能であり，術前 39 点から術後 89 点と有意に改善した．なかでも疼痛と日常生活動作で著しい改善を認めた（図 2）．

コンポーネント設置角度は，正面像で上腕骨コンポーネントは平均 2.5° 内反，側面像では平均 0.3° 前傾していた．尺骨コンポーネントは平均 9.1° 尻上がりとなった（図 3）．上腕骨コンポーネントに clear zone は認められなかった．X 線側面像での尺骨コンポーネント周囲の clear zone は 25 肘中 8 肘（全例滑車切痕部），loosening は 1 肘（尺骨コンポーネントステムに及ぶ clear zone）に認められた．Clear zone の層別内訳は尺骨コンポーネントとセメント間 8 肘，セメントと尺骨間 1 肘であった．

北海道大学　整形外科
* 信州大学　整形外科
**北海道整形外科記念病院

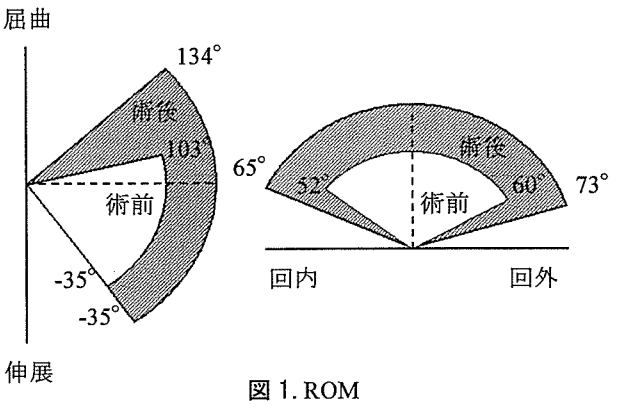

図 1. ROM

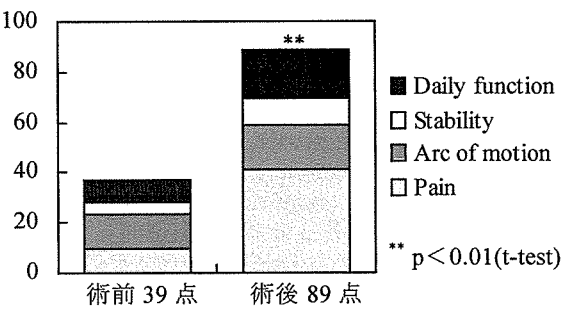

図 2. Mayo Elbow Performance Score

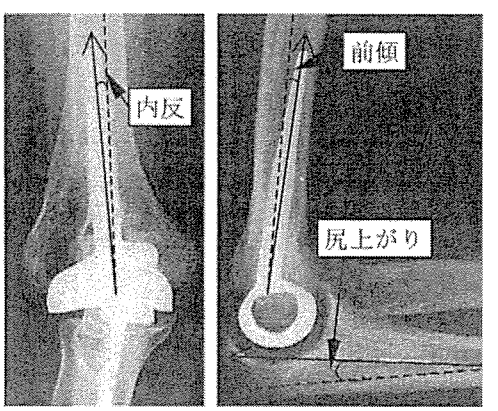

図 3. コンポーネント設置角度

25 肘中 4 肘（16%）で合併症が認められた．術中合併症として，上腕骨内顆骨折を 1 例に生じ，骨接合術を追加した．術後合併症としては，術後早期の脱臼・縫合部皮膚欠損・肘頭骨折がそれぞれ 1 例ずつ認められた．これらに対する対処法として，脱臼に対しては上腕三頭筋

と内側側副靭帯再建術を，縫合部皮膚欠損に対しては rotational flap を追加した．また clear zone が生じた 1 肘では術後軽微な外力による肘頭骨折を生じたため，骨接合術を施行したが骨癒合が得られず，最終的に尺骨コンポーネント再置換とプレートによる骨接合術を行った．

【症例】69 歳・女性．術前の肘関節 ROM は伸展-60°，屈曲 150° で，強い疼痛を伴った不安定性があり，ADL 上支障があったため，右人工肘関節置換術を施行した．術前 X 線所見では Larsen 分類 grade 4 と判断した．Mayo Score は 60 点, Fair であった (図 4)．術後 2 年 3 ヵ月時，X 線上 clear zone は認められるものの，伸展-30° ・屈曲 150°，Mayo Score も 100 点・Excellent に改善した (図 5)．

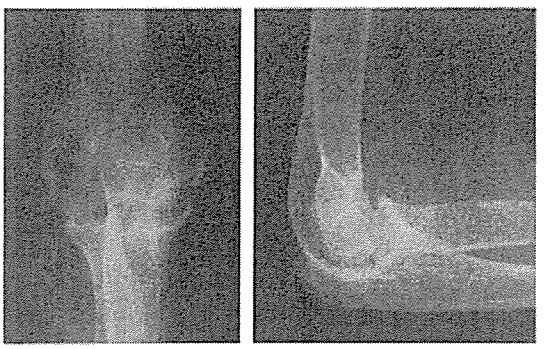

図 4. 術前 X 線

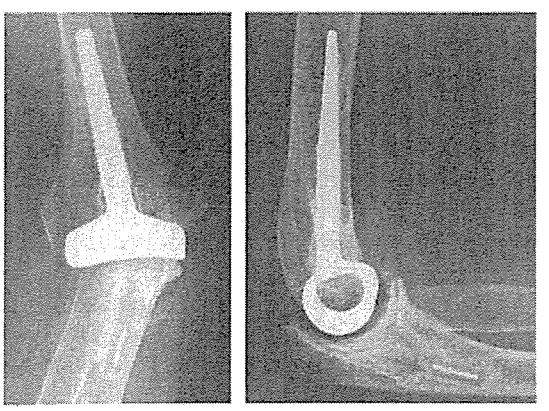

図 5. 術後 X 線

【考察】多関節障害のみられる RA 患者では肩関節，肘関節，手・指関節の変形，可動域制限や疼痛により，ADL は著しく制限されている．このような患者の中には肘関節障害が上肢機能障害の主因となっていることも多く，手術による肘関節機能の改善が上肢機能・ADL に与える効果は非常に大きいと考えられる．

当科では X 線所見上 Larsen 分類 grade 4 以上の関節破壊が進行した症例に対して，肘関節障害の改善を目的とし，人工肘関節置換術を行っている．そのなかでも，不安定性が比較的経度で，骨欠損の少ない症例に対しては，表面置換型の Kudo Elbow を使用し，1994 年以降は安定した結果が報告されている Kudo Elbow type 5 を用いている．

今回の調査では ROM において，屈曲は吉野ら [4]の述べる機能的可動域を獲得することができたが，術後も伸展制限は残存した．表面置換型では骨切除量をできるだけ少なくするために関節部分で延長が起こってしまうこと，前方軟部組織の拘縮，肘頭先端や肘頭窩の骨棘・セメントの遺残，尺骨コンポーネントの尻上がり設置がこの要因として考えられている [1]．我々の症例においても，尺骨コンポーネントは平均 9.1° 尻上がりに設置されており，このことは伸展制限が残存した要因の一つであったと考えている．

臨床所見では Mayo Elbow Performance Score の全ての項目において改善がみられたが，特に疼痛・日常生活動作項目における改善が大きく，著明な除痛効果・屈曲域の拡大による患者の満足度は高かった．

X 線上の clear zone・loosening の発生頻度に関しては，報告者によりさまざまであるが，我々の症例では 25 肘中 8 肘 (32%) に clear zone が，1 肘 (4%) で loosening が認められた．最も早いものでは術後 2 年でセメント周囲に clear zone が出現した症例もあったが，最終経過観察時では clear zone の拡大や臨床症状の悪化は認められず，clear zone がすぐに loosening に結びつくものではないと考えている．しかしながら，1 例ではあるが loosening が生じた後に，軽微な外力によって肘頭骨折を来たした症例もあり，X 線上変化が認められた症例については注意深い経過観察が必要であると思われた．

Clear zone・loosening が認められた 9 例において尺骨コンポーネントの種類・固定法に関して検討したところ，9 肘中 7 肘が all HDP type・セメント固定であり，all HDP type・セメント固定例では clear zone を生じる傾向にあると考えられた．

【まとめ】RA 肘に対して工藤式人工肘関節置換術を行い，中期経過観察期間ではあるが臨床上満足のいく結果を得た．長期成績の追跡が必要ではあるが，本法は肘関節機能を改善し得る有用な治療法であると考えられた．

文　献

1) 岩堀裕介　他：RA 肘に対する工藤式人工肘関節置換術の臨床成績と合併症．日肘研誌 9:35-36,2002.

2) Kudo H.,et al.:Total elbow arthroplasty with use of a nonconstrained humeral component inserted without cement in patients who have rheumatoid arthritis.J.Bone Joint Surg.81-A:1268-1280,1999.

3) Morrey,B.F.,et al.:Semiconstrained arthroplasty for the treatment of rheumatoid arthritis of the elbow. J.Bone Joint Surg.74-A:479-490,1992.

4) 吉野正昭　他：慢性関節リウマチに対する工藤式肘関節置換術の治療経験．日関外誌 XIV：321-326,1997.

Mod Rheumatol (2004) 14:184–186
DOI 10.1007/s10165-004-0289-2

CASE REPORT

**Hiroshi Horiuchi · Masashi Nawata · Tetsuyoshi Kamijo
Naoto Saito · Shigeyuki Wakitani · Seneki Kobayashi
Tominaga Shimizu · Hiroyuki Kato**

Locking of the knee caused by localized pigmented villonodular synovitis: a case report

Received: July 15, 2003 / Accepted: October 28, 2003

Abstract Pigmented villonodullar synovitis (PVS) occurs in two forms: diffuse PVS and localized pigmented villonodular synovitis. In this report, a 40-year-old woman presented with a history of recurrent episodes of knee locking and pain. Arthroscopy revealed a nodular pedunculated mass occupying the area anterior to the intercondylar notch of the femur. Histological examination of the tissue confirmed the diagnosis of PVS. After surgery, the patient's symptoms of pain and recurrent locking promptly resolved.

Key words Arthroscopy · Knee · Pigmented villonodular synovitis (PVS)

Introduction

Pigmented villonodullar synovitis (PVS) occurs in two forms: diffuse and localized (LPVS). The knee joint is the site most commonly affected, although lesions have been described in a variety of other joints. Most consider PVS to be a benign inflammatory process, whereas others think that the pathological characteristics of some lesions suggest a neoplastic condition.[1] We present a case of LPVS of the knee that caused it to lock recurrently. Arthroscopic procedures to remove the lesion were performed, and no recurrence was observed.

Case report

A previously healthy 40-year-old woman presented with a 1-year history of pain in her left knee. It began when the patient started to kneel and felt her left knee lock, preventing full extension. She saw her local physician immediately, who manipulated the knee into extension. Approximately 3 months after the initial injury, the patient again experienced locking of her left knee while running. During this second occurrence, the patient was unable to unlock her knee, and she visited her local physician for treatment. One week after her second injury, the patient visited our hospital. She had no history of remarkable swelling or hemarthrosis of the left knee joint.

Examination revealed a slight limp and restricted range of motion in the knee joint. There was no ligamentous abnormality, and she had no typical meniscus tear signs. No biochemical disorders in the blood examinations were seen. Radiographs did not reveal any abnormal shadows. However, magnetic resonance imaging (MRI) did reveal a mass in the anterior intercondylar space near the insertion of the anterior cruciate ligament. She had experienced both medial and lateral knee pain, which was exacerbated by squatting, standing, and walking. Prior to surgery, her symptoms worsened after prolonged standing, and she could not squat or fully extend her left knee because of pain.

Arthroscopy revealed a nodular pedunculated mass occupying the area anterior to the intercondylar notch of the femur (Fig. 1). The mass was round with a smooth surface and yellow-brown pigmentation. The remaining synovium was seen within the joint space, and all structures were noted to be normal. No other similar lesions were detected. The entire lesion was completely removed through the anteromedial portal. Histological examination of the lesion demonstrated the presence of multinucleated giant cells, hypercellularity, fibroconnective tissue, and pigmentation (Fig. 2). These features established the diagnosis of PVS.

The patient's symptoms of pain and recurrent locking promptly resolved. At her 7-month postoperative follow-up, the patient remains symptom-free and has returned to a low level of sports participation.

H. Horiuchi (✉) · M. Nawata · T. Kamijo · N. Saito · S. Wakitani · S. Kobayashi · T. Shimizu · H. Kato
Department of Orthopaedic Surgery, School of Medicine, Shinshu University, 3-1-1 Asahi, Matsumoto 390-8621, Japan
Tel. +81-263-37-2659; Fax +81-263-35-8844
e-mail: horiuchi@hsp.md.shinshu-u.ac.jp

Discussion

Pigmented villonodular synovitis occurs in large joints, bursa, or tendon sheaths. The etiology is unknown. It occurs in two forms: a diffuse pigmented villonodular synovitis involving the entire synovium or a localized pigmented villonodular synovitis.

The localized form of PVS is a rare pathological condition. The knee joint is most commonly affected, and the disease is generally characterized by the presence of a single pedunculated nodular lesion. The patient occasionally presents with various symptoms such as pain, swelling, or a palpable mass in the knee.[2,3] There are a few previous case reports of localized PVS lesions producing meniscal symptoms.[4–6] In the present case, prior to surgery the patient had a recurrence of her knee locking, such as might occur with a locking bucket handle tear of the meniscus.

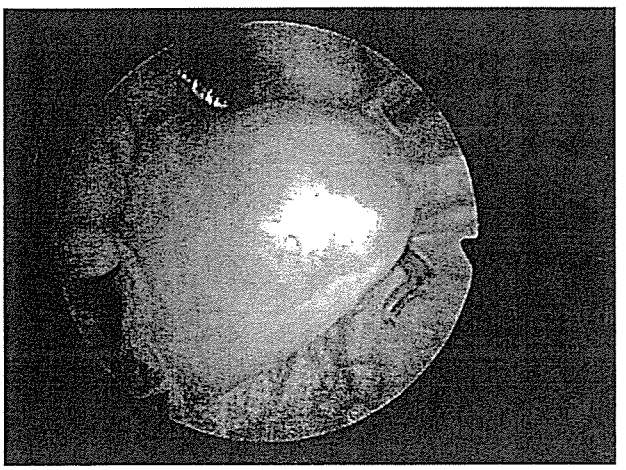

Fig. 1. Localized pigmented villonodular synovitis lesion located anterior to the intercondylar notch

Histologically, PVS is characterized by a fibrous stroma, proliferation of round histiocytic cells or spindle cells, and hemosiderin deposits in macrophages and synovium. The lesions are predominantly villous or nodular in appearance, and in some cases both are seen. The degree of pigmentation ranges from barely yellow to dark brown.[1]

Although radiographic findings are usually normal when examined in localized PVS, a soft tissue mass is occasionally seen. In patients with a diffuse form of PVS, bony changes are observed in a few cases and consist of cyst formations, cortical erosions, and osteopenia.[4,5] The MRI finding of a localized form of PVS is relatively specific, and the signal intensity is similar to that of the diffuse form of PVS, which is characterized by a hypointense area on both T1- and T2-weighted images. This pattern correlates with intralesional deposits of hemosiderin. However, this appearance is not specific for the localized form of PVS and can be confused with synovial chondromatosis or fibroxanthoma.[7]

The localized form of PVS has a good prognosis, in contrast to the diffuse form. Recurrence has been reported but appears to be uncommon.[1,8] Although there is a paucity of literature on localized PVS, arthroscopy can be used as an effective diagnostic method to identify localized PVS in the knee.[9–11]

Conclusions

We described a case of localized PVS of the knee presenting as a recurring locked meniscal tear in a 40-year-old woman. The patient was treated via arthroscopy to remove the mass, and the diagnosis was confirmed by histological findings. At her most recent follow-up, the patient is doing well, is symptom-free, and has returned to low-level sports participation.

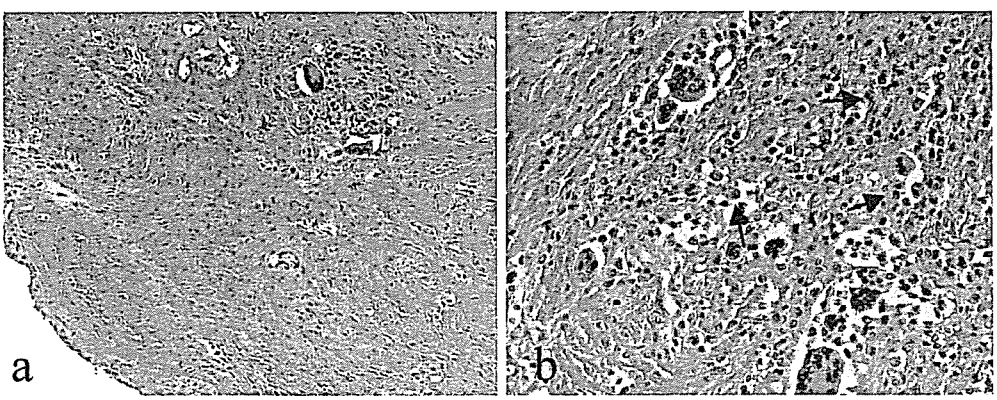

Fig. 2. **a** Pathology of localized pigmented villonodular synovitis demonstrates multinucleated giant cells, hypercellularity, and fibroconnective tissues. **b** At higher magnification, pigmentation (*arrows*) is seen to be present. H&E. **a** ×100, **b** ×200

References

1. Rao S, Vigoria V. Pigmented villonodular synovitis: giant-cell tumor of the tendon sheath and synovial membrane: a review of eighty-one cases. J Bone Joint Surg Am 1984;66:76–94.
2. Mancini GB, Lazzeri S, Bruno G, Pucci G. Localized pigmented villonodular synovitis of the knee. Arthroscopy 1998;14:532–6.
3. Hammer DS, Dienst M, Kohn DM. Arthroscopic treatment of tumor-like lesions of the knee joint: localized pigmented villonodular synovitis and ganglion cyst of the anterior cruciate ligament. Arthroscopy 2001;17:320–3.
4. Flandry F, McCann SB, Hughston JC, Kurtz DM. Roentgenographic findings in pigmented villonodular synovitis of the knee. Clin Orthop 1989;247:208–19.
5. Van Meter CD, Rowdon GA. Localized pigmented villonodular synovitis presenting as a locked lateral meniscal bucket handle tear: a case report and review of the literature. Arthroscopy 1994;9:309–12.
6. Williams AM, Myers PT. Localized pigmented villonodular synovitis: a rare cause of locking of the knee. Arthroscopy 1997;13:515–6.
7. Mandelbaum BR, Grant TT, Hartzman S, Reicher MA, Flannigan B, Bassett LW, et al. The use of MRI to assist in diagnosis of pigmented villonodular synovitis of the knee joint. Clin Orthop 1986;231:135–9.
8. Schwartz HS, Unni KK, Pritchard DJ. Pigmented villonodular synovitis: a retrospective review of affected large joint. Clin Orthop 1989;247:243–55.
9. Moskovich R, Parisien JS. Localized pigmented villonodular synovitis of the knee: arthroscopic treatment. Clin Orthop 1991;271:218–24.
10. Lee BI, Yoo JE, Lee SH, Min KD. Localized pigmented villonodular synovitis of the knee: arthroscopic treatment. Arthroscopy 1998;14:764–8.
11. Tatari H, Baran O, Lebe B, Kilic S, Manisali M, Havitcioglu H. Pigmented villonodular synovitis of the knee presenting as a popliteal cyst. Arthroscopy 2000;16:13.

PAPER

Quantitative MRI of the wrist and nerve conduction studies in patients with idiopathic carpal tunnel syndrome

S Uchiyama, T Itsubo, T Yasutomi, H Nakagawa, M Kamimura, H Kato

J Neurol Neurosurg Psychiatry 2005;**76**:1103–1108. doi: 10.1136/jnnp.2004.051060

See end of article for authors' affiliations

Correspondence to: Dr S Uchiyama, Director, Department of Orthopaedic Surgery, Suwa Red Cross Hospital, Suwa City, 392-8510, Nagano Prefecture, Japan; sigeharu-utiyama@suwa.jrc.or.jp

Received 1 August 2004
In revised form 24 November 2004
Accepted 1 December 2004

Objective: To correlate morphological findings of idiopathic carpal tunnel syndrome (CTS) with the function of the median nerve.

Methods: In this study, 105 wrists of 105 women patients with idiopathic CTS, and 36 wrists of 36 female volunteers were subjected to nerve conduction studies and MRI. Cross sectional area, signal intensity ratio, and the flattening ratio of the median nerve, carpal tunnel area, flexor tendon area, synovial area, and intersynovial space, and the palmar bowing of the transverse carpal ligament (TCL) were quantified by MRI and correlated with the severity of the disease determined by nerve conduction studies.

Results: Cross sectional areas of the median nerve, flexor tendons, and carpal tunnel, and the palmar bowing of the TCL of the CTS groups were greater than in the control group, but differences were not detected among the CTS groups for the area of the flexor tendons and the carpal tunnel. Enlargement, flattening, and high signal intensity of the median nerve at the distal radioulnar joint level were more significant in the advanced than in the earlier stages of the disease. Increase in palmar bowing of the TCL was less prominent in the most advanced group. Linear correlation between the area of the carpal tunnel and palmar bowing of the TCL was noted.

Conclusion: Severity of the disease could be judged by evaluating not only longitudinal changes of signal intensity and configuration of the median nerve, but also palmar bowing of the TCL. Increased palmar bowing of the TCL was found to be associated with an increase in the area of the carpal tunnel.

Idiopathic carpal tunnel syndrome (CTS) is the most common entrapment neuropathy in the upper extremity; however, its aetiology remains unclear. With the development of imaging techniques, new evidence related to the carpal tunnel has been reported.[1 2] Previous studies on the carpal tunnel using MRI compared the median nerves of patients with CTS with those of normal individuals, and determined the specific changes inside the carpal tunnel that determine diagnostic accuracy.[2 3] Proximal swelling, flattening, and high signal intensity of the median nerve on the T2 image and an increased bowing of the transverse carpal ligament (TCL) were regarded as the characteristic findings for idiopathic CTS.[2–8] However, results were not always consistent because of differences in sample size and the inclusion of individuals with various stages of the disease or of patients of both sexes. Furthermore, quantitative analysis of the structures inside the carpal tunnel, rather than the median nerve, is very limited, although they are probably related to the pathophysiology of idiopathic CTS.

In this study, we quantified the structures inside the carpal tunnel on MRI and correlated findings with nerve conduction studies in patients with idiopathic CTS to evaluate if disease severity had an effect on morphological changes. We investigated only women because idiopathic CTS is more often seen in women than men,[9] and differences in area of the flexor tendons and the carpal tunnel are known to exist between the sexes.[10 11]

MATERIALS AND METHODS

We prospectively studied 105 wrists of 105 consecutive women patients diagnosed with idiopathic CTS, and 36 wrists of 36 female volunteers. Exclusion criteria for this study were history of any surgery or wrist fracture of the affected hand, double crush injury, diabetes mellitus, gout, rheumatoid arthritis, or other systemic disease. Written informed consent was obtained from all subjects, and the hospital ethics committee approved the study protocol.

All subjects underwent clinical examination, nerve conduction studies, and MRI. Posterioanterior and lateral plain *x* ray films were taken of the affected wrist of the patients to check for bony abnormalities such as lunatomalacia, incorrect union of a distal radial fracture, bone tumour, or bony erosion. Clinical examination included Phalen's test, percussion test at the carpal tunnel, determination of area of sensory disturbance, Semmes-Weinstein monofilament test, and a pinch and grip strength test. Chronicity of the disease was determined based on the duration of numbness reported by the patients. The diagnosis of idiopathic CTS was made on the basis of medical history and physical examination. Nerve conduction studies were conducted using Neuropack MEB-5504 (Nihon Kohden, Tokyo, Japan) to determine motor distal latency (MDL) and sensory conduction velocity (SCV). Details of the measurement procedure have been reported previously.[12]

MRI of the carpal tunnel was performed on the affected hand of the patients and the right hand of the volunteers. The protocol for the MRI was as follows: field strength,1.5 Tesla (Toshiba VISART EX, Tokyo Japan); coil type, circular extremity coil (GPFLEX); arm wrist position was prone with the arm extended over the head, the forearm in pronation, wrist in neutral position and fingers extended; and imaging direction was the axial plane from the distal radioulnar joint to the carpometacarpal joint level. T1 weighted spin echo images and T2 weighted gradient echo images were obtained (repetition time 600 and 380 ms; echo time 18 and 15 ms for T1 and T2 respectively; section thickness, 3 mm; intersection space, 0.3 mm; number of signals acquired, 2 for T1 and 2.6

Abbreviations: CTS, carpal tunnel syndrome; MDL, motor distal latency; SCV, sensory conduction velocity; TCL, transverse carpal ligament